3-23-2023

Out-of-oven rapid synthesis of entropy stabilized oxides using radio frequency heating

L. K. Bhaskar

Jared Rapp

Ankush Nandi

A. K. Biswal

K. Z. Uddin
Rowan University

See next page for additional authors

Recommended Citation

Bhaskar, L.K., Rapp, J., Nandi, A., Biswal, A.K., Uddin, K.Z., Koohbor, B., Kumar, R. and Vashisth, A. (2023), "Out-of-oven rapid synthesis of entropy stabilized oxides using radio frequency heating", Journal of Materials Research and Technology, Vol. 24, pp. 1150-1161.

Available online at www.sciencedirect.com

jmr&t Journal of Materials Research and Technology

journal homepage: www.elsevier.com/locate/jmrt

Original Article

Out-of-oven rapid synthesis of entropy stabilized oxides using radio frequency heating

Lalith Kumar Bhaskar [a,b], *Jared Rapp* [c], *Ankush Nandi* [c], *Agni Kumar Biswal* [c], *Kazi Zahir Uddin* [d], *Behrad Koohbor* [d], *Ravi Kumar* [a,b,**], *Aniruddh Vashisth* [c,*]

[a] *Laboratory for High Performance Ceramics, Department of Metallurgical and Materials Engineering, Indian Institute of Technology Madras, Chennai 600036, India*

[b] *Ceramic Technologies Group, Centre of Excellence in Materials and Manufacturing for Futuristic Mobility, Indian Institute of Technology Madras (IIT Madras), Chennai 600036, India*

[c] *Department of Mechanical Engineering, University of Washington, Seattle, WA 98195, United States*

[d] *Department of Mechanical Engineering, Rowan University, Glassboro, NJ, 08028, United States*

ARTICLE INFO

Article history:
Received 7 January 2023
Accepted 8 March 2023
Available online 14 March 2023

Keywords:
RF heating
ESOs
ESO-Carbon composites
Oxides
Entropy stabilized oxides

ABSTRACT

Entropy stabilized oxides (ESOs) are a new class of stable hybrids and single phase metal oxides made from multiple ions with material properties somewhere between the constituent oxides, or occasionally entirely new properties. One of the limitations of ESOs is their energy-intensive fabrication process, which has resulted in slow development and scale-up of new ESOs. In this work, we present a novel energy-efficient ESO synthesis method that uses the ability of carbonaceous materials to heat rapidly in response to radio frequency (RF) fields in 1–200 MHz range. Using carbon fibers and graphene as RF susceptors, synthesis of $(Mg_{0.2}Co_{0.2}Ni_{0.2}Cu_{0.2}Zn_{0.2})O$ is achieved through RF-initiated combustion synthesis with heating rates of 203 °C/s at 20 W of input power. This method reduces the formation time of ESOs to less than a minute, allowing for much more efficient fabrication. The corresponding morphology and composition of the as-synthesized ESO-carbon fiber and ESO-graphene were studied using extensive spectroscopy and characterization. Additionally, single carbon fibers coated with ESO were tested for tensile strength and modulus; little change in mechanical properties was observed as compared to pristine fibers. This work opens an exciting frontier for the rapid synthesis of ESO-carbon composites using RF heating as a non-contact, rapid, and efficient manufacturing process.

* Corresponding author. Department of Mechanical Engineering, University of Washington, Seattle, WA 98195, United States
** Corresponding author. Laboratory for High Performance Ceramics, Department of Metallurgical and Materials Engineering, Indian Institute of Technology Madras, Chennai 600036, India
E-mail addresses: nvrk@iitm.ac.in (R. Kumar), vashisth@uw.edu (A. Vashisth).
https://doi.org/10.1016/j.jmrt.2023.03.060

1. Introduction

Entropy stabilized oxide (ESO) are an exciting class of ceramics that differ from traditional oxides; these ceramics can contain multiple cations distributed throughout the bulk while still maintaining a single primary phase [1]. Researchers have found rock salt ESOs with multiple cations binding to oxygen [1,2] with transitions metals such as $(Mg_{0.2}Co_{0.2}Ni_{0.2}Cu_{0.2}Zn_{0.2})O$, $(CoCrFeMnNi)_3O_4$, etc. [1,3,4]. ESOs that are commonly termed as high entropy oxides have garnered a significant amount of interest as they have shown excellent properties in energy storage [5], low electrical conductivity [6,7], low thermal conductivity [8], dielectric [9,10], magnetic [11], optical [12], catalytic [13] and mechanical [8,14] applications.

ESOs maintain a primary single-phase on the basis of configurational entropy, where configurational entropy is a measure of the entropy gained by the atomic mixing and variation in the ESO composition. The primary limiting factor in ESO stability is lattice strain; when multiple cations are present in a lattice, the overall lattice must distort in order to accommodate the atomic radii differences between the different cation types. Therefore, the greater the differences in atomic radii of the cations, the greater the resulting lattice strain [15]. Another requirement for stability is that the cations present in the ESO should have equal or similar oxidation states to maximize the overall stability [1,16]. Interestingly, for certain cation combinations, this configurational entropy is able to overcome the lattice distortion introduced by the presence of multiple cations, resulting in a single-phase ESO [17].

A unique characteristic of ESOs is that their material properties can be customized by adjusting their chemical compositions. This can be achieved by adjusting ratios and types of cation types [1,3,6]. By adjusting the chemistry of ESOs, a wide range of tunability can be realized in electromagnetic [18–21], conductivity [22], thermal [23,24], and catalytic [25–28] properties. The current manufacturing processes of these oxides rely on the use of high-temperature ovens or furnaces that are energy and time intensive [1–3,29]. As such, the expensive nature of synthesis hinders the mass and rate of production, discovery, and scaling-up of these novel materials. Recently, Mao et al. proposed a solution combustion synthesis (SCS) of ESOs [30] that combines constituent metal nitrates with a fuel such as urea or glycine. The solution converts into a gel-like precursor as the water evaporates. When the gel reaches a temperature of ~180 °C, a self-propagating combustion reaction occurs instantaneously, bringing the mixture's temperature above the ESO synthesis temperatures [31]. However, high-temperature oven-based heating and SCS approach require significant energy input, thus, limiting large-scale production since the rate of heating bounds the method.

Recently, it was discovered that radio frequency (RF) fields (1–200 MHz) could be used for volumetric heating of carbonaceous materials with minimal power inputs [32–34]. This method can be used for out-of-oven rapid fabrication of materials through an energy-efficient, non-contact method of heating [35–38]. An advantage of non-contact heating is that the carbon additive can be either continuous or discrete. Carbonaceous materials that interact with RF and heat include carbon sheets, carbon fibers, carbon nanotubes, graphene, and carbon black [32]. Interestingly, carbon-based fillers can also be added to the oxides to improve the material's charge transport, mechanical strength, and cyclability [39,40].

This paper aims to explore the viability of utilizing a carbon filler for faster and more energy-efficient activation of solution combustion synthesis. In this investigation, we show that RF fields can be used for patterning ESOs on carbonaceous materials. Inside-to-outside rapid heating can be achieved using RF fields to initiate SCS. Carbon fibers and graphene nanoparticles were used as carbonaceous susceptors for SCS of $(Mg_{0.2}Co_{0.2}Ni_{0.2}Cu_{0.2}Zn_{0.2})O$ ESOs. While RF heating is a non-contact heating method, we also evaluate SCS using direct current (DC) heating for patterning ESOs on carbon fibers. The structure of the synthesized carbon-ESO composites is characterized using various diffraction methods and studied for mechanical properties. Our works establishes RF heating as a novel non-contact and energy-efficient method for rapid synthesis of ESO and ESO-composites.

2. Methods and characterization

This section is divided into two parts; the first part outlines the synthesis and sample preparation for ESOs using RF and DC heating, and the second section details the experimental procedures carried out for sample characterization. Fig. 1 shows a detailed overview of the ESO synthesis initiated by various carbonaceous materials, including Radio Frequency heating and DC Heating.

2.1. *Sample preparation*

2.1.1. *Precursor solution*

A master batch of fuel-oxidizer precursor solution was made and used for all experiments. The metal nitrates are dissolved in water in an equimolar fashion to create the precursor solution. Glycine is then added to the solution in a molar ratio of 0.5:1 glycine to nitrate salts. The chemicals used in these experiments were Magnesium Nitrate Hexahydrate (BeanTown, 98%), Cobalt (II) Nitrate Hexahydrate (Aldon Corporation, ≥99%), Nickel Nitrate Hexahydrate (Aldon Corporation, ≥99%), Copper (II) Nitrate Hemipentahydrate (BeanTown, ≥98%), Zinc (II) Nitrate Hexahydrate (Avantor, ≥99%), and Glycine (BeanTown, ≥99%). The solution was then mixed via magnetic stirrer for 1 h at room temperature, resulting in the salts and glycine to be fully dissolved. In this mixture, glycine is the fuel, and the nitrate salts are the oxidizer for the combustion reaction.

2.1.2. *Hot plate SCS of ESO*

Once mixed, the precursor solution was transferred to a separate beaker, which was then placed on a hot plate. The hot plate temperature was set to 180 °C, and the solution was left to heat up and boil off excess water. Eventually, the solution's viscosity dramatically increased, followed quickly by the combustion reaction initiated by the fuel-oxidizer mixture producing ESO.

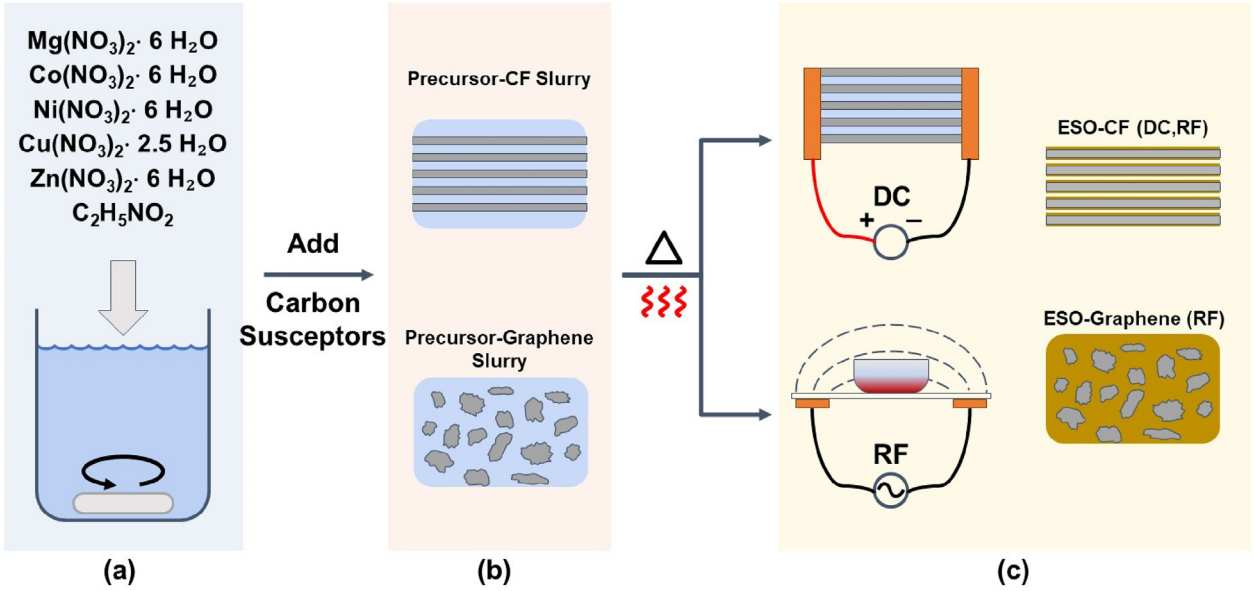

Fig. 1 – ESO Synthesis process can be sub-divided into three steps: (a) mixing all the nitrates with DI water and glycine; (b) impregnation or dispersion of carbonaceous materials with the solution; (c) synthesis and patterning ESO on carbonaceous materials through DC and RF heating.

2.1.3. *Synthesis of ESOs from radio frequency heating*

Once the precursor solution was thoroughly mixed, the ESO solution was transferred to a Petri dish containing the carbon fiber (CF) tow of T700 (Toray, Japan) in submerged condition. These experiments utilized 12K T700 carbon fiber tows, with each fiber having a 7 μm nominal diameter. The system was baked at 80 °C for 2 h to drive off excess water from the solution then RF heating was carried out on this sample to get ESOs on CFs. The RF heating system consists of a signal generator (Rigol Inc., DSG815) and a 500 W amplifier (Prana R&D, GN500D) that were used to supply RF power to the applicator via a 50Ω coaxial cable. A FLIR infrared camera (FLIR Systems Inc., A700) was used to record the temperature during the reaction. A frequency of 144 MHz was used with 20 W of input RF power for the synthesis of ESO. A more detailed description of the RF setup can be found in Refs. [41,42].

2.1.4. *Synthesis of ESOs from DC heating*

Another more proven out-of-oven heating method of carbonaceous material is direct current (DC) joule heating, which utilizes the electrical resistance of carbon to generate heat [43,44]. However, this method requires physical contact, making it challenging to achieve continuous processing [41]. DC heating was used to pattern ESO on carbon fibers; the preparation steps are discussed in detail next. A mixture of precursor solution was transferred to a ceramic boat, and a CF tow of T700 (Toray, Japan) was then submerged into the solution ensuring good impregnation. The combustion boat was baked at 80 °C for a period of 2 h to drive off excess water from the solution. Next, conductive metal tape was applied to the ends of the saturated CF tow for DC heating. A EPSCO GFL Filtered DC Power Supply was used to provide DC power (10–20 W) for heating the impregnated CF tow to initiate combustion reaction. A FLIR infrared camera was used to record the temperature as a function of time.

2.2. *Sample analysis*

The morphology, crystal structure, and mechanical properties of Entropy stabilized oxide (ESO) and Entropy stabilized oxide – Carbon fiber (ESO-CF) specimens were evaluated experimentally. This section provides an overview of the experimental methods.

2.2.1. *X-ray diffraction (XRD)*

Room-temperature X-ray diffraction (XRD) was conducted using a Bruker D8 Discover (Germany) with 2θ ranging from 10° to 100°, step size of 0.01° and a scan speed of 1 s/step. The accelerating voltage and current were kept at 40 kV and 35 mA. These measurements were then normalized between 0 and 1 for ease of XRD shape comparison.

2.2.2. *Scanning electron microscopy (SEM)*

Samples were imaged using Thermofischer - Apreo S (USA) coupled with an energy-dispersive X-ray spectrometer (EDS) from Bruker X Flash (Germany). The atomic fractions were determined from the elemental mapping of the sample obtained from 5 different spots.

2.2.3. *BET surface area*

To study the surface area of the ESO-CF samples, BET surface analysis was conducted and Brunauer-Emmett Teller (BET) equation was used to calculate the surface area. Nitrogen adsorption-desorption isotherms were obtained at −196 °C using 3020 - Tristar II, Micromeritics, after degassing the sample at 150 °C for 12 h.

2.2.4. Raman spectroscopy

The Raman spectra of the samples were analyzed using a LabRAM HR800 Raman spectrometer from Horiba Jobin-Yvon (Japan) equipped with an Olympus BX41 microscope having an objective lens magnification of 50 × . A He–Ne laser source of 632 nm laser with 1800 groves/mm grating was used in the range of 200–2000 cm^{-1}. The sampling period for each measurement was 120 s. These spectra were then normalized between 0 and 1 for ease of spectra shape comparison. In samples containing carbon fiber, the intensity of the *D*-band (~1350 cm^{1}) was divided by the intensity of the *G*-band (~1580 cm^{1}) to determine the I_D/I_G defect ratios for the analyzed carbon structures.

2.2.5. X-ray photoelectron spectroscopy (XPS)

All XPS analysis was conducted with a Kratos Axis-Ultra DLD spectrometer with a monochromatized Al Kα X-ray and a low energy electron flood gun for charge neutralization. The X-ray spot size for these acquisitions was on the order of 700 × 300 μm. The analytical chamber pressure was maintained under 5 × 10^{-9} Torr during spectral acquisition. The pass energy for the survey and detailed spectra (composition) was 80 eV. For the high-resolution spectra, the pass energy was 20 eV. The take-off angle (i.e., the angle between the sample normal and the input axis of the energy analyzer) was 0 (0-degree take-off angle ~ 100 Å sampling depth). The Kratos Vision2 software program was used to determine peak areas and to calculate elemental compositions from peak areas. CasaXPS was used to peak fit the high-resolution spectra. A Shirley background was used for the high-resolution spectra, and all binding energies were referenced to the C–C bonds at 285.0 eV.

2.2.6. Inductively coupled plasma mass spectrometry (ICP-MS)

Samples underwent microwave-assisted (MARS 5, CEM Matthews, NC) digestion prior to inductively coupled plasma – mass spectrometry (ICP-MS) analysis for: Mg, Co, Ni, Cu, and Zn with terbium (Tb) added as recovery internal standard. The ICP-MS instrument (Agilent 7900-CE; Santa Clara, CA) has a collision reaction cell, which was used in He mode to eliminate polyatomic interferences (US EPA 6020A Rev1, 2007).

2.2.7. Single fiber mechanical testing

Single fiber mechanical tests were performed to characterize the tensile response of the pristine (commercially available T700 carbon fiber, Toray Industries, Inc. Tokyo), and ESO coated carbon fibers. The test protocol followed ASTM C1557-20 standardized tensile test method for sample preparation, mounting, and testing of single fiber specimens. A single fiber was separated from the fiber bundle and mounted in a thin paper tab using an epoxy adhesive. The epoxy was given enough time to ensure it was completely cured. Full curing was required to ensure no fiber pull-out occurred during the tensile test. Fig. 2a shows a schematic of a single fiber sample mounted in the paper tab. The mounting tab contains a longitudinal slot (created with a laser cutter) to maintain a fixed gage length of 25 mm. A laser diffraction method based on the "Fraunhofer Single Slit Diffraction" principle was performed in a dark room setup to measure the fiber cross-sectional area (see Fig. 2b). The single fiber diameter (d) is calculated using the following relation,

$$d\ (\mu m) = \frac{2 \times \lambda(nm) \times s(m)}{\delta_f(mm)} \quad (1)$$

where, λ is the known laser wavelength, and *s* is the distance between the screen and fiber. In this equation, the separation between the first adjacent pair of minima is represented by δ_f. After inserting the paper tab in the load frame, the final stage of the test preparation included carefully burning the thinnest parts of the tab with a soldering iron at mid-gage length. Tensile testing was conducted in an Instron load frame equipped with a 10 N load cell (Fig. 2c).

The tensile load was applied at a constant displacement rate of 1 mm/min until failure. A pneumatic gripping system was used to verify the alignment of the fiber specimen with the loading direction. Forty independent measurements were performed for each specimen type.

3. Results and discussion

In this work, the ESO oxides [$(Mg,Co,Ni,Cu,Zn)_{0.2}O$] were synthesized using RF and DC heating, along with the more traditional method of combustion synthesis (on a hot plate). In the rapid fabrication of ESOs using RF fields and DC heating, the oxide precursor solution was patterned on the carbon fibers that acted as heat generators during the synthesis process. The ESO synthesized using a hot plate was used as a reference. In the hot plate synthesis method, the entire volume of the reactive mixture was uniformly preheated to the solvent's boiling point, and consequently, the solution mixture was maintained at 180 °C where the solvent evaporates. In the final stage, a sudden increase in temperature occurs due to the ignition of the fuel, which results in the formation of ESO. In order to calculate the adiabatic temperature generated during the combustion reaction and to determine the equilibrium reactant products formed, the reducing/oxidizing valences of the redox mixture are considered. The overall redox reaction for the synthesis of the ESO would be as shown in Eq. (2).

$$0.2\ Co(NO_3)_2 + 0.2\ Cu(NO_3)_2 + 0.2\ Ni(NO_3)_2 + 0.2\ Zn(NO_3)_2 + 0.2\ Mg(NO_3)_2 + 1.5\varphi\ C_2H_5NO_2 + (5/2)\ [\varphi - 1]\ O_2 \rightarrow (MgNiCoCuZn)O + 3\varphi\ CO_2 + (1 + 0.75\varphi)\ N_2 + 3.75\varphi\ H_2O \quad (2)$$

The adiabatic combustion temperature (T_{ad}) is significant as the ESO stabilizes into a single phase $(MgNiCoCuZn)_{0.2}O$ oxide at a temperature of 848 °C for the fuel/oxidizer used in this study (as shown in Supplementary Information). Therefore, for the fuel/oxidizer ratio used in this study, an initial temperature of ~150 °C is sufficient to initiate a combustion reaction to generate a single-phase ESO. This concept was exploited in synthesizing ESO using RF and DC heating. A more detailed explanation has been summazied in the Supplementary Information. The carbon source provided the initial heating in the RF and DC synthesis method, which triggered the secondary combustion reaction. The reactions and temperatures were systematically monitored, and the observations are compiled in this section.

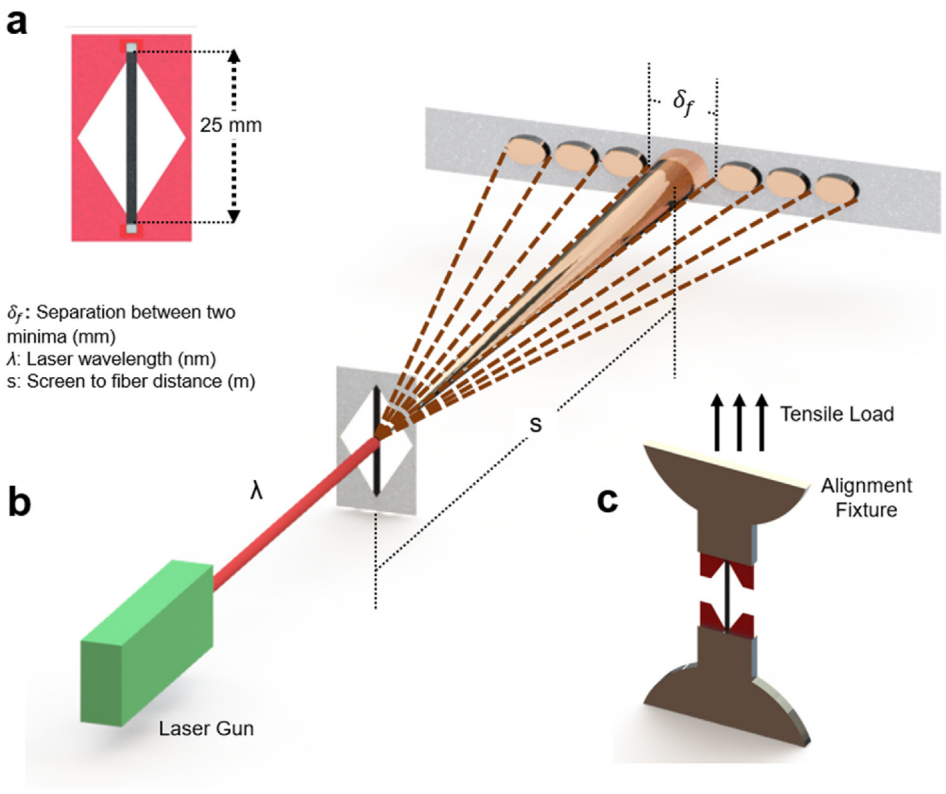

Fig. 2 – (a) Schematic of a single fiber in a mounting tab. (b) The fiber diameter is measured by laser diffraction method. (c) The sample is loaded under a tensile load.

An infrared (IR) camera monitored ESO synthesis process by RF and DC heating, and the thermal profile generated is shown in Fig. 3. Excess water evaporates during the first 20–30 s for both RF and DC synthesis, transitioning the cation solution to a blue-colored gel. This is the state where all precursor ions become well-packed on the surface of carbonaceous heat susceptors while the water evaporates from the system. As shown in Fig. 3a for RF-initiated ESO synthesis, a short spike reaching up to 700 °C at 35 s and rapid ESO formation are observed in the next 5 s. For the DC heated specimens (Fig. 3b), the global temperatures reach 300–350 °C during the combustion reaction; continuous ESO formation is seen during this time. The heating rates during the combustion step are 203 °C/s for RF heating and 73 °C/s for DC heating, therefore RF synthesis of ESO requires much less time as compared to DC heating. Fig. 3 shows that during RF heating, the combustion of precursor requires a fraction of time compared to DC heating and happens more uniformly. Additionally, we experimented with graphene-embedded precursor and found that non-contact RF heating can successfully be

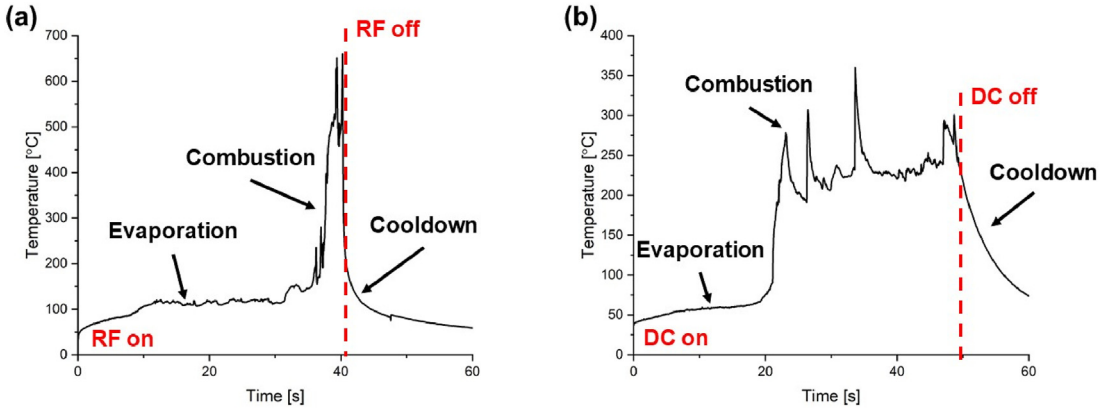

Fig. 3 – Thermal profile recorded by the FLIR camera during the ESO synthesis using (a) RF fields and (b) DC heating.

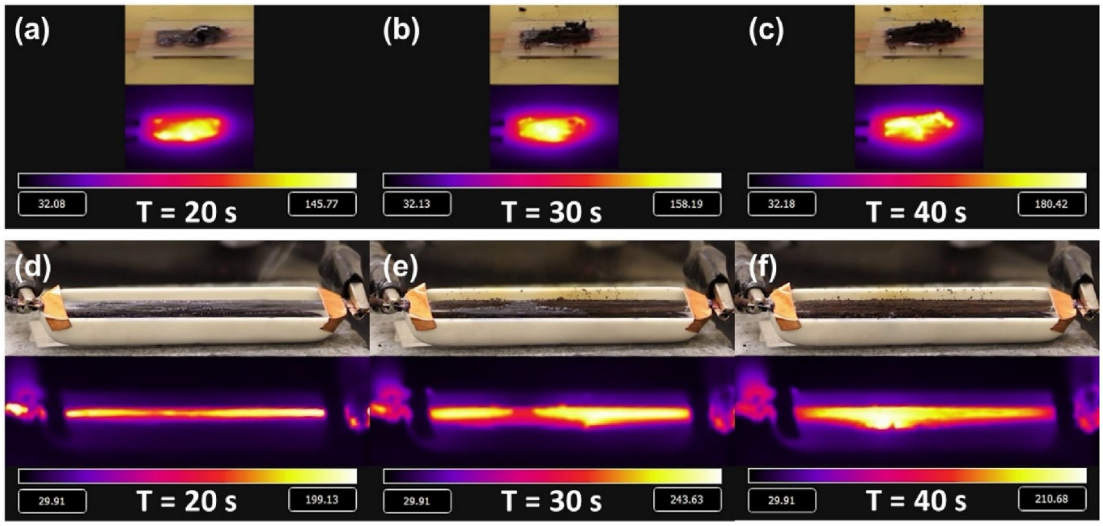

Fig. 4 – Thermal and corresponding visual image of ESO synthesis on carbon fibers during the last 20 s of the reaction initiated by (a–c) the non-contact RF and (d–f) DC heating methods.

used to synthesize ESO. The synthesized powder using CF and graphene as heat susceptors was analyzed using imaging and elemental analysis to confirm the formation of ESOs.

During the synthesis, visual recordings were also carried out to complement the thermal imaging captured by the IR camera; these can be seen in Supplementary Information (SI videos 1 and 2). Snapshots for these videos at different intervals are shown in Fig. 4 for RF and DC heating synthesis of ESO-CF. The advantage of RF heating over DC heating is its non-contact heating interaction with CF samples. As the reaction progresses (Fig. 4a–c), a flaky coating of ESO can be seen forming on the fibers. Similarly, as seen in Fig. 4d–f, ESO forms on the CF during the DC heating process. Interestingly, a combustion front is seen close to the electrodes for DC-heated specimens, and the reaction propagates from both ends of the electrodes toward the center (SI video 2).

Supplementary video related to this article can be found at https://doi.org/10.1016/j.jmrt.2023.03.060

SEM images of carbon fibers show continual ESO coating (Fig. 5) and uniform metal cation distribution (Fig. 6). Visual inspection of ESO-CF samples shows that ESO-CF synthesized through RF heating has a much uniform and thicker coating than ESO-CF synthesized through DC heating. Fig. 6 shows the SEM-EDS for ESO-CF synthesized by RF heating and found that all metal ions were uniformly distributed in the ESO phase,

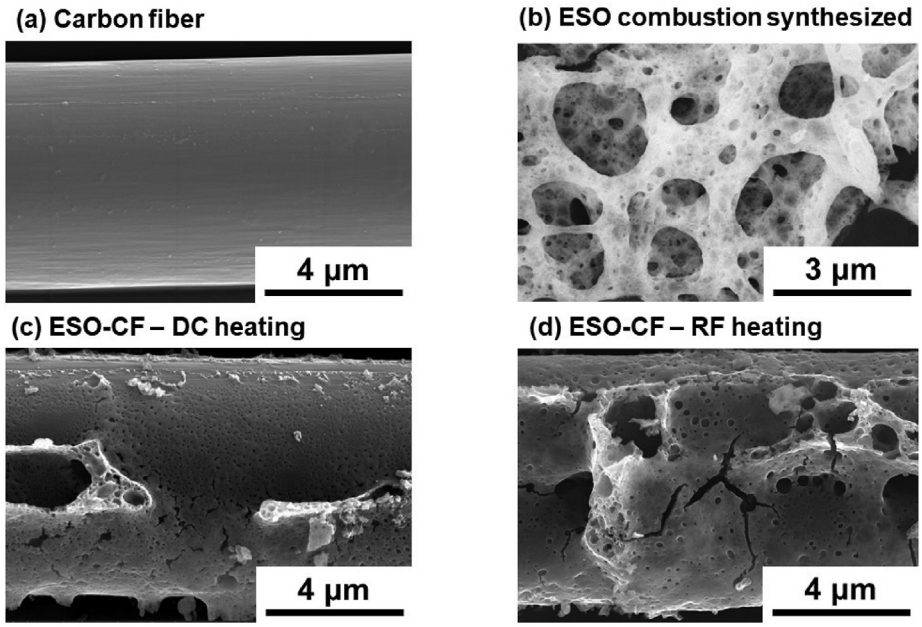

Fig. 5 – SEM image of the carbon fiber and ESO-coated carbon fiber synthesized through DC and RF heating.

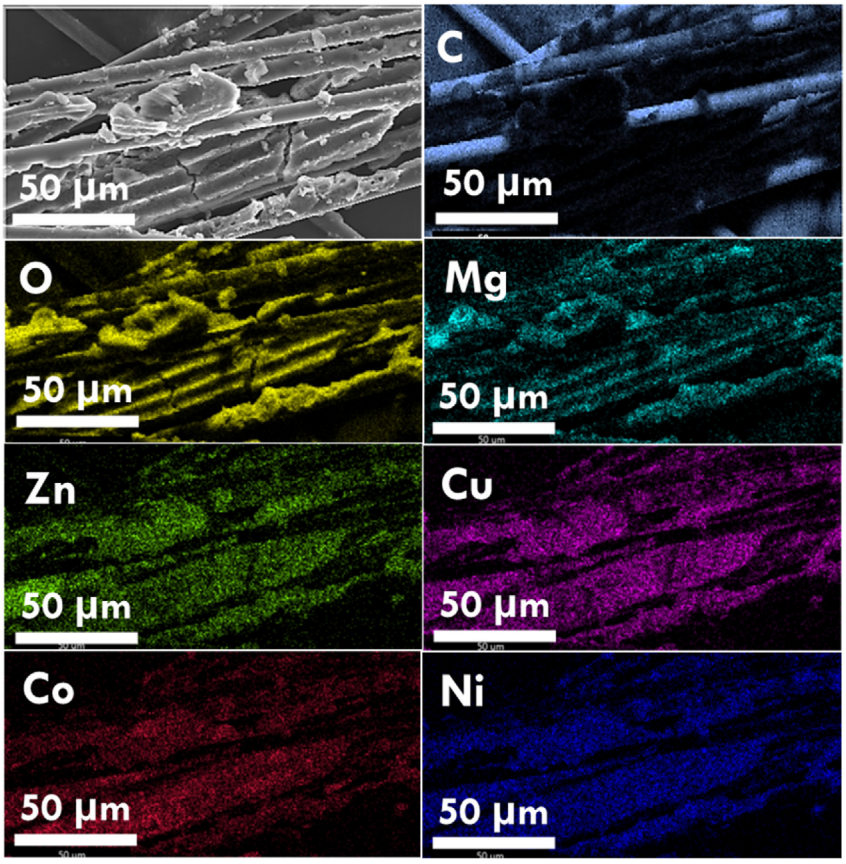

Fig. 6 – Top left image panel shows the SEM image of CF coated with ESO from RF heating method. EDS readings show the distribution of five cations in the ESO patterned on CFs: Mg, Co, Ni, Cu, and Zn, along with oxygen and carbon from fibers.

confirming a uniform coating. This uniform coating of ESOs on CFs suggests that RF heating facilitates the packing of the ionic precursors in a controlled manner during the slow evaporation stage that took 30 s (Fig. 3). SEM-EDS of CF-ESO synthesized from DC heating are shown in Figure SI 1, and the cation distribution is less uniform compared to RF-synthesized CF-ESOs. During the combustion synthesis using RF and DC heating, the gel that converts to ESO crystals bridges multiple CFs; these microscopic phenomena result in ceramic bridges between fibers observed in SEM images.

Additionally, ESOs were synthesized by incorporating varying concentrations of graphene particles from 0.1-1 wt% in the precursor. While DC heating synthesis of such slurry requires a percolated network, this is particularly not important for RF heating-driven ESO synthesis; RF heating can be achieved at much lower concentrations of nanofillers [32]. Interestingly, a porous structure evolves from RF synthesis of ESO-graphene, as shown in Fig. 7. These particles were examined using SEM, and it was observed that ESOs covered the graphene nanoparticles completely. This suggests that

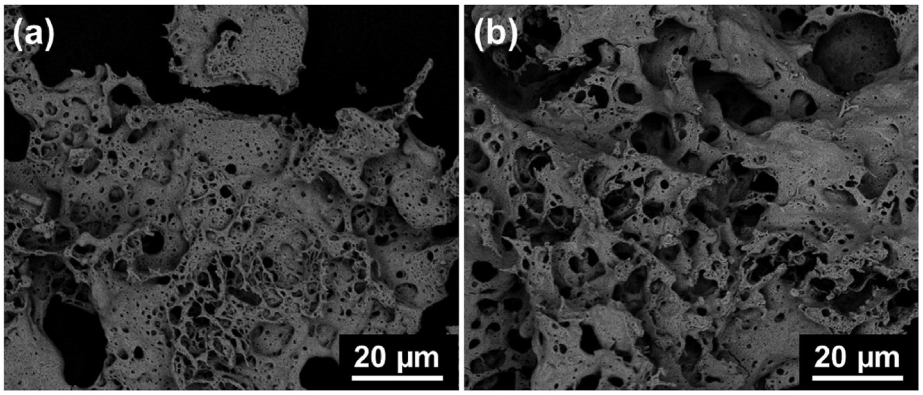

Fig. 7 – ESO fabricated by RF heating with 0.1 wt% graphene and 1 wt% graphene.

high surface area carbonaceous nanomaterials bind effectively with ESOs in the presence of RF heating due to volumetric heating. The average diameter of these macropores was measured to be 1.8 ± 0.5 μm using ImageJ analysis software on the SEM images. However, it should be noted that pores with larger diameters contribute little to the specific surface area.

The surface area of the fabricated ESOs using different methods was measured using BET. The specific surface area increases when ESOs are synthesized on carbon fibers by DC and RF heating combustion syntheses. However, it remains below the specific surface area of hot-plate ESO synthesis without carbon fibers (Table 1). It was observed that the ESO-CF produced with DC heating resulted in a higher specific surface area than when produced by RF heating. The difference in surface area between the DC and RF synthesized could be explained by the adhesion of the ESO particles on fiber surfaces. The SEM analysis (Fig. 5) shows that the RF-synthesized ESO-CF fibers had a thicker and more uniform coating on the fibers compared to the DC-synthesized fibers. This results in higher mass per unit length for ESO-CF synthesized by RF heating, lowering the specific surface area compared to DC-synthesized ESO-CF. In contrast, the ESO particles adhered to the DC synthesized ESO-CF fibers are non-uniform and randomly arranged on the CF surface. The latter, contributes to the increase in specific surface area. The low surface area of the synthesized ESO and ESO-CF composites exemplifies that the particles are not mesoporous. The BET surface area measurement method is only sensitive to mesoporous particles with a pore size of 2–50 nm.

The crystal structure and phase purity of the synthesized particles were studied using X-ray diffraction. The formation of ESOs from different synthesis routes was confirmed by XRD analysis. XRD patterns in Fig. 8 shows no evidence of the presence of secondary phases and virtually identical primary phase crystal structures for ESOs synthesized using DC and RF heating with respect to traditional SCS hot plate heating. The ESO synthesized using both DC and RF heating of carbon fiber contained the same diffraction angle peaks as ESO synthesized with traditional SCS hot plate heating. The peaks at $2\theta \approx 36^{\circ}$ & 42° correspond to the (111) and (200) planes of the rock-salt crystal structure. Also, all the patterns exhibit one significant peak at $2\theta \approx 25–28^{\circ}$, generally corresponding to the (200) plane diffraction of graphite crystalline structure [45]. The other noticeable phenomenon is the peak broadening of the XRD peaks which indictaes that the ESO formed are nano crystalline. The crystallite size was calculated using the Williamson-Hall plot and was estimated to be 35 ± 11 nm for the ESO sample, and 24 ± 9 nm and 26 ± 9 nm for the ESO-CF samples synthesized through DC and RF heating, respectively. From the crystallite size calculation, we observe that the ESO coating on the CF fibers is indeed nanosized which remains unaffected by the synthesis method.

Raman spectroscopy was employed to study the structure of the synthesized ESOs (Fig. 9a). It was observed that the ESO-CF samples had the same intensity peak near 550 cm^{-1} as the hot-plate ESO (Fig. 9a), indicating that the DC and RF based heating methods resulted in similar crystal growth to hot-plate heating for SCS. D and G bands were also visible in both the DC and RF ESO-CF samples. The I_D/I_G defect ratio

Table 1 – BET surface area results for ESO, carbon fibers, ESO-CF prepared by DC and RF heating.

Sample	Surface Area [m^2/g]
ESO	32
Carbon Fiber	1
ESO-CF: RF Heating	4
ESO-CF: DC Heating	10

(Figure SI 2) reduced as a consequence of heating and ESO coating compared to uncoated CF specimens (1.166), more so for the DC specimen (1.016) than the RF specimen (1.133). Though the bonding characteristic and the defect chemistry were understood using Raman spectroscopy, the stoichiometry of the synthesized ESO needs to be measured. For this, the oxidation state of each element was measured using XPS.

The stability of ESOs synthesized by these two methods was also confirmed by the electronic structures of ions from XPS analysis. The presence of carbon, oxygen, and nitrogen can be seen for all specimens analyzed, along with +2 oxidation state characteristic peaks for Co, Ni, Zn, Cu, Mg (Fig. 8b and Table SI2); the presence of these cations is also verified from their EDS mapping. Note that after the ESO coating, the oxygen content increases significantly. The increased oxygen content indicates the presence of stable ESO crystals. The electronic states +2 for Mg and Ni are observed with highly stable packing structures showing oxides with octahedron surroundings, these can be seen from XPS analysis in Fig. 9b with peaks at ~48 eV and 853 eV for Mg and Ni, respectively. The formation of nanocrystals suggests that the ions like Cu and Co have more stable ionic state oxides, which is also confirmed by the peaks at 932 eV and 778 eV, respectively [46]. XPS and SEM-EDS provides surface composition analysis, these techniques are not able to capture the weight compositions. Therefore, we carried out ICP-MS to measure the weight compositions. We found that the average weight composition of Mg, Co, Ni, Cu, Zn, and C are 2.8%, 7.2%, 7.1%,

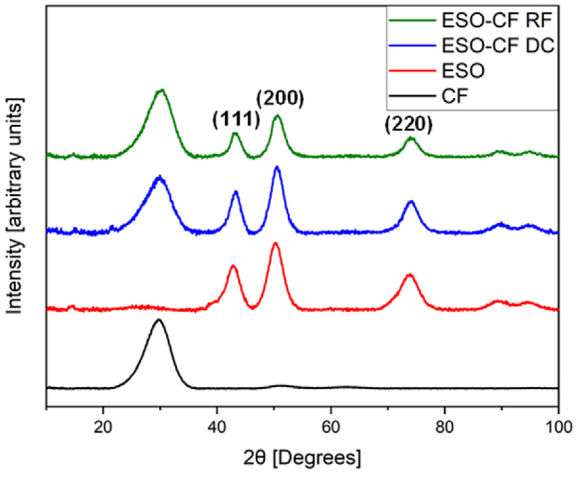

Fig. 8 – XRD patterns of ESO-CF synthesized using RF and DC heating, ESO synthesized by hot-plate combustion synthesis, and as received carbon fibers.

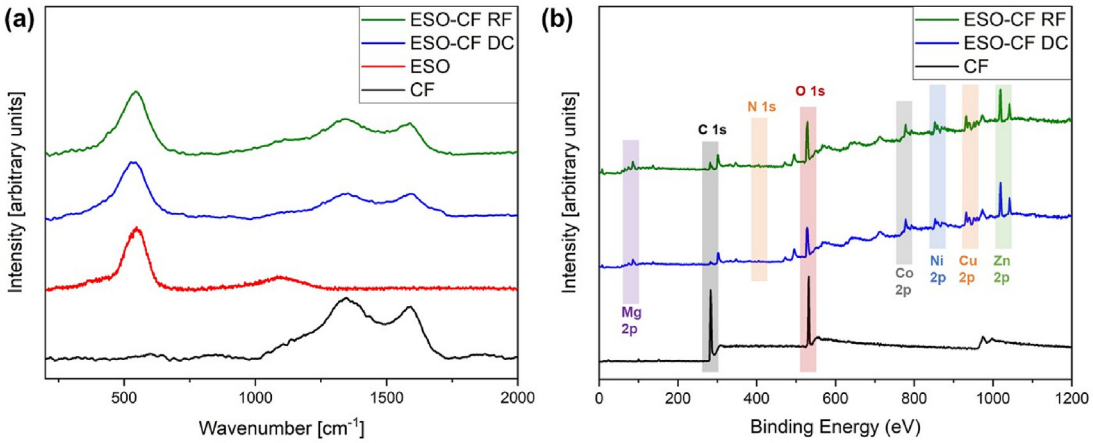

Fig. 9 – Results of (a) Raman spectroscopy and (b) XPS characterization of ESO-CF specimens synthesized by RF and DC heating.

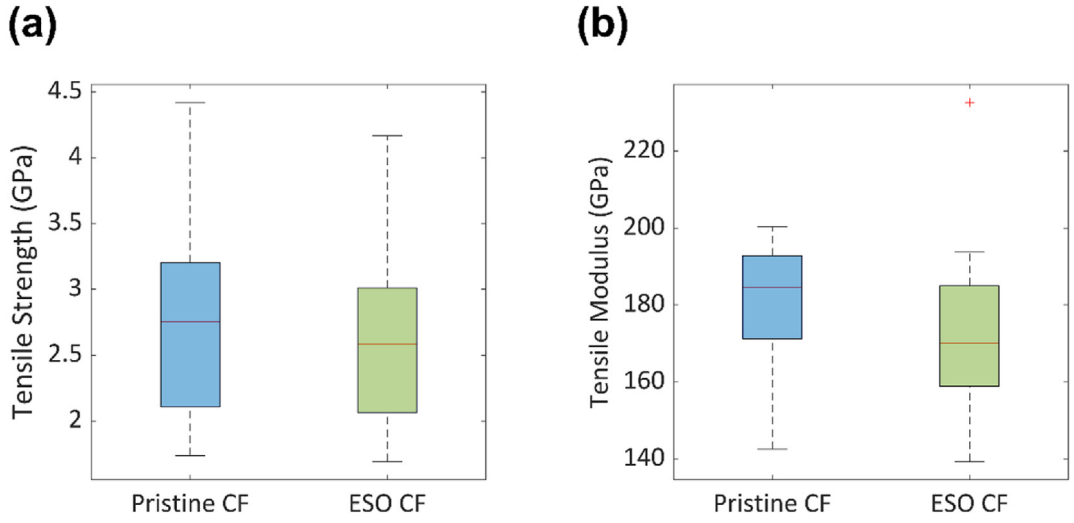

Fig. 10 – (a) Tensile strength, and (b) tensile modulus of pristine and ESO coated carbon fibers.

7.6%, 7.6%, and 67.9%, respectively. Detailed results are tabulated in Supplementary Information SI Table 2.

Finally, the mechanical performances of pristine and ESO-CF were investigated using the aforementioned single fiber test procedure. Specimens that failed near the grippers were discarded from strength and modulus measurements. As shown in Fig. 10a, an average tensile strength of 2.8 GPa was measured for pristine CFs, whereas the strength decreased slightly to an average value of 2.6 GPa for ESO CFs. The tensile moduli of the two conditions were also determined as 180.8 GPa and 173.2 GPa for pristine and ESO CFs, respectively (Fig. 10b). A decrease in the tensile strength and modulus of less than 7% and 4.2%, respectively, were observed in the ESO fibers. This slight drop in fiber modulus and strength can be attributed to the rapid high-temperature synthesis of ESOs on CF surfaces, possibly leading to the development of residual stresses in the material.

4. Conclusion

For the first time, a new method for producing ESO-carbon composites has been demonstrated using out-of-oven electromagnetic heating using radio frequencies in the range of 1–200 MHz at low input power (less than 25 W). ESOs were synthesized using RF and DC heating of carbonaceous materials responding to electromagnetic fields and direct current. ESO was synthesized and deposited on the CFs. Heating rates

of 203 °C/s are achieved from the combustion synthesis of ESO-CFs with only 20 W input powers. The inside-to-outside nature of the RF heating produced ESO-CF composite with a uniform coating without using energy-expensive large ovens in less than a minute. Apart from rapid manufacturing and energy efficiency, this provides an excellent opportunity for synthesizing multifunctional materials where ESO-CF can be used for structural and energy storage applications. Using RF heating, ESO-graphene nanocomposites were also synthesized with varying nanofiller concentrations. The non-contact nature of RF heating makes RF-synthesis of ESO-graphene more desirable as compared to DC heating, which requires direct contact with ESO-graphene slurry. Characterization of ESOs synthesized by RF heating closely resembles conventionally synthesized ESOs. Both carbonaceous materials (CFs and graphene) bind well with ESOs during RF heating; therefore, depending on the size and shape of nanomaterials, RF parameters, various architectures of ESO ceramic morphologies can be generated for targeted applications. Mechanical testing of single fibers in a pristine state and ESO-coated show a minimal drop in tensile modulus and strength. For future studies, machine learning [47,48] can be used to develop efficient RF heating protocols for ESO synthesis using various carbonaceous fillers.

Declaration of competing interest

The authors declare that they have no known competing financial interests or personal relationships that could have appeared to influence the work reported in this paper.

Acknowledgments

Part of this work was conducted at the Molecular Analysis Facility, a National Nanotechnology Coordinated Infrastructure (NNCI) site at the University of Washington, which is supported in part by funds from the National Science Foundation (awards NNCI-2025489, NNCI-1542101), the Molecular Engineering & Sciences Institute, and the Clean Energy Institute. We thank the Environmental Health Laboratory in the Department of Environmental and Occupational Health Sciences at the University of Washington for providing ICP-MS services. The authors would also like to acknowledge the funding received from the Institute of Eminence Research Initiative Project on Materials and Manufacturing for Futuristic Mobility (Project No:SB20210850MMMHRD008275) from IIT Madras. Single fiber tests were performed at the Advanced Materials and Manufacturing Institute (AMMI) at Rowan University. The authors wish to gratefully acknowledge Dr. James Newell and Mr. William Beck at Rowan University for their helpful discussions and assistance with the single fiber tests.

Appendix A. Supplementary data

Supplementary data to this article can be found online at https://doi.org/10.1016/j.jmrt.2023.03.060.

REFERENCES

[1] Rost CM, Sachet E, Borman T, Moballegh A, Dickey EC, Hou D, et al. Entropy-stabilized oxides. Nat Commun Dec. 2015;6(1):8485. https://doi.org/10.1038/ncomms9485.
[2] Chen K, Pei X, Tang L, Cheng H, Li Z, Li C, et al. A five-component entropy-stabilized fluorite oxide. J Eur Ceram Soc Sep. 2018;38(11):4161–4. https://doi.org/10.1016/j.jeurceramsoc.2018.04.063.
[3] Dąbrowa J, Stygar M, Mikuła A, Knapik A, Mroczka K, Tejchman W, et al. Synthesis and microstructure of the (Co,Cr,Fe,Mn,Ni) 3 O 4 high entropy oxide characterized by spinel structure. Mater Lett Apr. 2018;216:32–6. https://doi.org/10.1016/j.matlet.2017.12.148.
[4] Yang Z-M, Zhang K, Qiu N, Zhang H-B, Wang Y, Chen J. Effects of helium implantation on mechanical properties of (Al 0.31 Cr 0.20 Fe 0.14 Ni 0.35)O high entropy oxide films. Chin Phys B Apr. 2019;28(4):46201. https://doi.org/10.1088/1674-1056/28/4/046201.
[5] Kiat Y, Vortman Y, Sapir N. High entropy oxides for reversible energy storage. Nat Commun Dec. 2018;9(1):3400. https://doi.org/10.1038/s41467-018-05774-5.
[6] Bérardan D, Franger S, Dragoe D, Meena AK, Dragoe N. Colossal dielectric constant in high entropy oxides. Phys Status Solidi RRL Apr. 2016;10(4):328–33. https://doi.org/10.1002/pssr.201600043.
[7] Stygar M, Dąbrowa J, Moździerz M, Zajusz M, Skubida W, Mroczka K, et al. Formation and properties of high entropy oxides in Co-Cr-Fe-Mg-Mn-Ni-O system: novel (Cr,Fe,Mg,Mn,Ni)3O4 and (Co,Cr,Fe,Mg,Mn)3O4 high entropy spinels. J Eur Ceram Soc Apr. 2020;40(4):1644–50. https://doi.org/10.1016/j.jeurceramsoc.2019.11.030.
[8] Musicó BL, Gilbert D, Zac Ward T, Page K, George E, Yan J, et al. The emergent field of high entropy oxides: design, prospects, challenges, and opportunities for tailoring material properties. Apl Mater Apr. 2020;8(4):40912. https://doi.org/10.1063/5.0003149.
[9] Zhou S, Pu Y, Zhang Q, Shi R, Guo X, Wang W, et al. Microstructure and dielectric properties of high entropy Ba(Zr0.2Ti0.2Sn0.2Hf0.2Me0.2)O3 perovskite oxides. Ceram Int Apr. 2020;46(6):7430–7. https://doi.org/10.1016/j.ceramint.2019.11.239.
[10] Pu Y, Zhang Q, Li R, Chen M, Du X, Zhou S. Dielectric properties and electrocaloric effect of high-entropy (Na 0.2 Bi 0.2 Ba 0.2 Sr 0.2 Ca 0.2)TiO 3 ceramic. Appl Phys Lett Nov. 2019;115(22):223901. https://doi.org/10.1063/1.5126652.
[11] Meisenheimer PB, Kratofil TJ, Heron JT. Giant enhancement of exchange coupling in entropy-stabilized oxide heterostructures. Sci Rep Dec. 2017;7(1):13344. https://doi.org/10.1038/s41598-017-13810-5.
[12] Sarkar A, Loho C, Velasco L, Thomas T, Bhattacharya SS, Hahn H, et al. Multicomponent equiatomic rare earth oxides with a narrow band gap and associated praseodymium multivalency. Dalton Trans 2017;46(36):12167–76. https://doi.org/10.1039/C7DT02077E.
[13] Li H, Zhu H, Zhang S, Zhang N, Du M, Chai Y. Nano high-entropy materials: synthesis strategies and catalytic applications. Small Struct Nov. 2020;1(2):2000033. https://doi.org/10.1002/sstr.202000033.
[14] Gild J, Samiee M, Braun JL, Harrington T, Vega H, Hopkins PE, et al. High-entropy fluorite oxides. J Eur Ceram Soc Aug. 2018;38(10):3578–84. https://doi.org/10.1016/j.jeurceramsoc.2018.04.010.
[15] Salian A, Mandal S. Entropy stabilized multicomponent oxides with diverse functionality – a review. Crit Rev Solid State Mater Sci Mar. 2022;47(2):142–93. https://doi.org/10.1080/10408436.2021.1886047.

[16] Delgado-Mellado N, Ayuso M, Mar Villar-Chavero M, García J, Rodríguez F. Synthesis and characterizations of (Mg, Co, Ni, Cu, Zn)O high-entropy oxides. SN Appl Sci Aug. 2021;3(8):733. https://doi.org/10.1007/s42452-021-04724-z.
[17] Bhaskar LK, Nallathambi V, Kumar R. Critical role of cationic local stresses on the stabilization of entropy-stabilized transition metal oxides. J Am Ceram Soc May 2020;103(5):3416–24. https://doi.org/10.1111/jace.17029.
[18] Vinnik DA, Zhivulin VE, Trofimov EA, Starikov AY, Zherebtsov DA, Zaitseva OV, et al. Extremely polysubstituted magnetic material based on magnetoplumbite with a hexagonal structure: synthesis, structure, properties, prospects. Nanomaterials Apr. 2019;9(4):559. https://doi.org/10.3390/nano9040559.
[19] Vinnik DA, Trukhanov AV, Podgornov FV, Trofimov EA, Zhivulin VE, Starikov AYu, et al. Correlation between entropy state, crystal structure, magnetic and electrical properties in M-type Ba-hexaferrites. J Eur Ceram Soc Sep. 2020;40(12):4022–8. https://doi.org/10.1016/j.jeurceramsoc.2020.04.036.
[20] Musicó B, Wright Q, Zac Ward T, Grutter A, Arenholz E, Gilbert D, et al. Tunable magnetic ordering through cation selection in entropic spinel oxides. Phys. Rev. Mater. Oct. 2019;3(10):104416. https://doi.org/10.1103/PhysRevMaterials.3.104416.
[21] Mao A, Xiang H-Z, Zhang Z-G, Kuramoto K, Zhang H, Jia Y. A new class of spinel high-entropy oxides with controllable magnetic properties. J Magn Magn Mater Mar. 2020;497:165884. https://doi.org/10.1016/j.jmmm.2019.165884.
[22] Bérardan D, Franger S, Meena AK, Dragoe N. Room temperature lithium superionic conductivity in high entropy oxides. J Mater Chem 2016;4(24):9536–41. https://doi.org/10.1039/C6TA03249D.
[23] Li F, Zhou L, Liu J-X, Liang Y, Zhang G-J. High-entropy pyrochlores with low thermal conductivity for thermal barrier coating materials. J. Adv. Ceram. Dec. 2019;8(4):576–82. https://doi.org/10.1007/s40145-019-0342-4.
[24] Braun JL, Rost CM, Lim M, Giri A, Olson DH, Kotsonis GN, et al. Charge-induced disorder controls the thermal conductivity of entropy-stabilized oxides. Adv Mater Dec. 2018;30(51):1805004. https://doi.org/10.1002/adma.201805004.
[25] Chen H, Fu J, Zhang P, Peng H, Abney CW, Jie K, et al. Entropy-stabilized metal oxide solid solutions as CO oxidation catalysts with high-temperature stability. J Mater Chem 2018;6(24):11129–33. https://doi.org/10.1039/C8TA01772G.
[26] Xu H, Zhang Z, Liu J, Do-Thanh C-L, Chen H, Xu S, et al. Entropy-stabilized single-atom Pd catalysts via high-entropy fluorite oxide supports. Nat Commun Dec. 2020;11(1):3908. https://doi.org/10.1038/s41467-020-17738-9.
[27] Albedwawi SH, AlJaberi A, Haidemenopoulos GN, Polychronopoulou K. High entropy oxides-exploring a paradigm of promising catalysts: a review. Mater Des Apr. 2021;202:109534. https://doi.org/10.1016/j.matdes.2021.109534.
[28] Deng C, Wu P, Zhu L, He J, Tao D, Lu L, et al. High-entropy oxide stabilized molybdenum oxide via high temperature for deep oxidative desulfurization. Appl Mater Today Sep. 2020;20:100680. https://doi.org/10.1016/j.apmt.2020.100680.
[29] Jiang S, Hu T, Gild J, Zhou N, Nie J, Qin M, et al. A new class of high-entropy perovskite oxides. Scr. Mater. Jan. 2018;142:116–20. https://doi.org/10.1016/j.scriptamat.2017.08.040.
[30] Mao A, Xiang H-Z, Zhang Z-G, Kuramoto K, Yu H, Ran S. Solution combustion synthesis and magnetic property of rock-salt (Co0.2Cu0.2Mg0.2Ni0.2Zn0.2)O high-entropy oxide nanocrystalline powder. J Magn Magn Mater Aug. 2019;484:245–52. https://doi.org/10.1016/j.jmmm.2019.04.023.
[31] Chick LA, Pederson LR, Maupin GD, Bates JL, Thomas LE, Exarhos GJ. Glycine-nitrate combustion synthesis of oxide ceramic powders. Mater Lett Sep. 1990;10(1–2):6–12. https://doi.org/10.1016/0167-577X(90)90003-5.
[32] Vashisth A, Upama ST, Anas M, Oh J-H, Patil N, Green MJ. Radio frequency heating and material processing using carbon susceptors. Nanoscale Adv 2021. https://doi.org/10.1039/D1NA00217A.
[33] Anas M, Mustafa MM, Vashisth A, Barnes E, Saed MA, Moores LC, et al. Universal patterns of radio-frequency heating in nanomaterial-loaded structures. Appl Mater Today Jun. 2021;23:101044. https://doi.org/10.1016/j.apmt.2021.101044.
[34] Sarmah A, Morales MA, Srivastava A, Upama S, Nandi A, Henry TC, et al. Interfacial carbon fiber–matrix interactions in thermosetting composites volumetrically cured by electromagnetic fields. Composer Part Appl Sci Manuf Jan. 2023;164:107276. https://doi.org/10.1016/j.compositesa.2022.107276.
[35] Gruener JT, Vashisth A, Pospisil MJ, Cardenas Camacho A, Oh J-H, Sophiea D, et al. Local heating and curing of carbon nanocomposite adhesives using radio frequencies. J Manuf Process Oct. 2020;58:436–42. https://doi.org/10.1016/j.jmapro.2020.08.039.
[36] Sweeney CB, Moran AG, Gruener JT, Strasser AM, Pospisil MJ, Saed MA, et al. Radio frequency heating of carbon nanotube composite materials. ACS Appl Mater Interfaces Aug. 2018;10(32):27252–9. https://doi.org/10.1021/acsami.8b06268.
[37] Oh JH, George GW, Martinez AD, Moores LC, Green MJ. Radio frequency heating of PEDOT:PSS. Polymer Sep. 2021;230:124077. https://doi.org/10.1016/j.polymer.2021.124077.
[38] Mason MJ, Coleman BJ, Saha S, Mustafa MM, Green MJ. Graphene signatures: identifying graphite and graphene grades via radio frequency heating. Carbon Sep. 2021;182:564–70. https://doi.org/10.1016/j.carbon.2021.06.046.
[39] Zhou H, Zhang L, Zhang D, Chen SQ, Coxon PR, He X, et al. A universal synthetic route to carbon nanotube/transition metal oxide nano-composites for lithium ion batteries and electrochemical capacitors. Sci Rep Dec. 2016;6(1):37752. https://doi.org/10.1038/srep37752.
[40] Kupila R, Lappalainen K, Hu T, Romar H, Lassi U. Lignin-based activated carbon-supported metal oxide catalysts in lactic acid production from glucose. Appl Catal Gen Feb. 2021;612:118011. https://doi.org/10.1016/j.apcata.2021.118011.
[41] Vashisth A, Healey RE, Pospisil MJ, Oh JH, Green MJ. Continuous processing of pre-pregs using radio frequency heating. Compos Sci Technol Jul. 2020;195:108211. https://doi.org/10.1016/j.compscitech.2020.108211.
[42] Vashisth A, Upama ST, Anas M, Oh J-H, Patil N, Green MJ. Radio frequency heating and material processing using carbon susceptors. Nanoscale Adv 2021;3(18):5255–64. https://doi.org/10.1039/D1NA00217A.
[43] Dong Q, Hong M, Gao J, Li T, Cui M, Li S, et al. Rapid synthesis of high-entropy oxide microparticles. Small Mar. 2022;18(11):2104761. https://doi.org/10.1002/smll.202104761.
[44] Wellekötter J, Bonten C. Influence of the contacting on the resistance heating of carbon fiber reinforced thermoplastics. 2020, 020057. https://doi.org/10.1063/5.0029567.
[45] Onck PR, van Merkerk R, Raaijmakers A, De Hosson J ThM. Carbon layer structures and thermal conductivity of graphitized carbon fibers. J Mater Sci 2012;47(6):2882–2890, Mar. https://doi.org/10.1007/s10853-011-6118-z.

[46] Thiem J, Cole DP, Dubey U, Srivastava A, Ashraf C, Henry TC, et al. Hidden transformations in entropy-stabilized oxides. J Eur Ceram Soc 2021;41(13):6660–6669, Oct. https://doi.org/10.1016/j.jeurceramsoc.2021.06.014.
[47] Tao H, Wu T, Aldeghi M, Wu TC, Aspuru-Guzik A, Kumacheva E. Nanoparticle synthesis assisted by machine learning. Nat Rev Mater Aug. 2021;6(8):701–16. https://doi.org/10.1038/s41578-021-00337-5.
[48] Thiem J, et al. Using data science to locate nanoparticles in a polymer matrix composite. Compos Sci Technol Feb. 2022;218:109205. https://doi.org/10.1016/j.compscitech.2021.109205.